*International Journal of Thermophysics, Vol. 15, No. 1, 1994*

# The Transport Properties of Ethane. II. Thermal Conductivity

**V. Vesovic,[1] W. A. Wakeham,[1] J. Luettmer-Strathmann,[2] J. V. Sengers,[2] J. Millat,[3] E. Vogel,[4] and M. J. Assael[5]**

*Received July 13, 1993*

A new representation of the thermal conductivity of ethane is presented. The representative equations are based upon a body of experimental data that have been critically assessed for internal consistency and for agreement with theory in the zero-density limit and in the critical region. The representation extends over the temperature range from 100 K to the critical temperature in the liquid phase and from 225 K to the critical temperature in the vapor phase. In the supercritical region the temperature range extends to 1000 K for pressures up to 1 MPa and to 625 K for pressures up to 70 MPa. The ascribed accuracy of the representation varies according to the thermodynamic state from ±2% for the thermal conductivity of the dilute gas near room temperature to ±5% for the thermal conductivity at high pressures and temperatures. Tables of the thermal conductivity, generated by the relevant equations, at selected temperatures and pressures and along the saturation line are also provided.

**KEY WORDS:** ethane; *n*-alkanes; transport properties; thermal conductivity.

## 1. INTRODUCTION

This paper is a continuation of our study of the transport properties of ethane. In the first part of this work [1] a representation for the viscosity of ethane was developed, whereas here we present the results for the

[1] IUPAC Transport Properties Project Center, Department of Chemical Engineering and Chemical Technology, Imperial College, London SW7 2BY, United Kingdom.
[2] Institute for Physical Science and Technology, University of Maryland, College Park, Maryland 20742, U.S.A.
[3] TECHRO e. V., Platz der Freundschaft 1, D-18059 Rostock, Germany.
[4] Fachbereich Chemie, Universität Rostock, D-18051 Rostock, Germany.
[5] Faculty of Chemical Engineering, Aristotle University, 54006 Thessaloniki, Greece.



0195-928X/94/0100-0033$07.00/0 

thermal conductivity. The aim of this study, which has been carried out under the auspices of the IUPAC Subcommittee on Transport Properties, is to continue the development of the representations of the transport properties of industrially important fluids.

There have been a number of correlations developed for the thermal conductivity of ethane over the last 20 years [2–5]. The earlier ones [2, 3] have since become obsolete both because a plethora of new experimental data was published in the 1980s and significant advances have been made in the understanding of the theory of thermal conductivity. The most recent correlation [5], covering a wide range of thermodynamic states, has been developed after a critical evaluation of the available data only 2 years ago. Nevertheless, it was felt that owing to the most recent developments, improvements are possible in certain regions of thermodynamic space. First new thermal conductivity data of high claimed accuracy have been published [6, 7]. The data cover regions of low density [6] and the vicinity of the critical point [7], which are the thermodynamic regions where our theoretical understanding is best [8–11]. Thus, the new data can be used in conjunction with the theory to improve substantially the representation of the thermal conductivity [10, 12]. Second, we believe that the latest theoretical developments concerning the behavior of the thermal conductivity in the zero-density limit [10, 13] and around the critical point [7, 11] allow a more secure analysis of the available experimental data than has been possible hitherto. Finally, as mentioned in part I of this work (the preceding paper) [1], a new, non-classical equation of state, valid in a region around the critical point, is now available [14].

The structure of the following sections is similar to that presented in part I for the viscosity [1]. A brief summary of the theory and the procedures used to develop the representation of the thermal conductivity is given, together with the coefficients and the functional forms of the resulting correlation. In general, most of the methodology is common with that used for other fluids and the reader is referred to our publication on carbon dioxide for further details [12].

## 2. METHOD

The methodology of analyzing the thermal conductivity data is, in general, similar to that used for the analysis of the viscosity data described in part I of this work [1]. For completeness and for further subsequent reference, we summarize the major points pertaining to the thermal conductivity. Thus, as for viscosity, it is customary [12, 15], for both fundamental and practical reasons, to decompose the thermal conductivity

$\lambda(\rho, T)$ of the fluid as a function of the density, $\rho$, and the temperature, $T$, into the sum of three contributions,

$$\lambda(\rho, T) = \lambda_0(T) + \Delta\lambda(\rho, T) + \Delta_c\lambda(\rho, T) = \bar{\lambda}(\rho, T) + \Delta_c\lambda(\rho, T) \qquad (1)$$

Here $\lambda_0$ is the thermal conductivity in the zero-density limit, $\Delta\lambda$ an excess thermal conductivity, and $\Delta_c\lambda$ a critical enhancement. It is also useful to define the background contribution $\bar{\lambda}$ as the sum of the first two terms in Eq. (1). The advantage of this approach, in developing the thermal conductivity correlation, is that it is possible to use both theoretical and experimental information to treat some of the contributions independently. Thus, it is possible to examine some of the available experimental data with respect to the most modern theory and to confirm their internal consistency. Furthermore, in the zero-density limit and around the critical point, theoretical studies have suggested appropriate functional forms for the representation of experimental data [7, 12].

In order to perform such an analysis, one must make use of experimental data over as wide a range of thermodynamic states as possible. Appendix I (Table AI) lists all the available sources of data on the thermal conductivity of ethane [6, 7, 16–43] and indicates the range covered and the method of measurement for each publication. In the same way as for viscosity, a critical analysis of all these data has been undertaken to define the primary data sets for each contribution to Eq. (1). The requirements for the primary thermal-conductivity data are the same as those for the viscosity data and they are described in part I of this work.

For the purposes of the analysis, the experimental thermal conductivity data must be available at specified temperatures and densities. The measurements are usually performed at specific temperatures, $T$, and pressures, $P$. In order to be entirely consistent, it is necessary to evaluate the density of the fluid from the temperature and pressure reported by experimentalists by means of a single equation of state (EOS). For this purpose we have employed the same EOS that we did for the analysis of viscosity. To summarize, the most recent classical EOS for ethane [5] has been used outside the critical region and a new parametric crossover EOS [14] has been employed in the critical region. The switching between the two EOS has been performed along the rectangular boundary in the temperature–density plane given by $302.5\ \text{K} \leqslant T \leqslant 316\ \text{K}$, $3.82\ \text{mol} \cdot \text{L}^{-1} \leqslant \rho \leqslant 8.65\ \text{mol} \cdot \text{L}^{-1}$ [14].

In subsequent sections we follow the same general strategy as employed for analysis of the viscosity data. Thus, we treat each contribution separately and analyze the primary data by means of the best available theoretical guidance. Independent representations are then developed for

each term in Eq. (1), which, when combined, give the global correlation for the thermal conductivity of ethane over a wide range of temperature and pressure. Throughout this work the temperature is in units of Kelvin in terms of IPTS-68, the pressure in units of MPa, the density in units of $\text{mol} \cdot \text{L}^{-1}$, and the thermal conductivity in units of $\text{mW} \cdot \text{m}^{-1} \cdot \text{K}^{-1}$.

## 3. THE ZERO-DENSITY LIMIT

The thermal conductivity of a fluid in the zero-density limit, $\lambda_0$, is an experimentally accessible quantity. Thus, it is possible to analyze $\lambda_0$ independently of other terms in Eq. (1) [10]. Although the existence of a well-developed kinetic theory [8, 9] in the same limit gives some guidance as to the form of the correlation, the interpretation of the theoretical results is not as straightforward as it was for viscosity. The major difference is that for the thermal conductivity, exchange of energy between translational and internal degrees of freedom plays a more prominent part. Hence, the theoretical analysis, compared with that for viscosity, has to take into account a number of additional cross sections pertaining to the relaxation and diffusion of the internal energy and its interaction with the translational energy.

Recent studies have shown [10, 12, 44] that, for molecules possessing only rotational degrees of freedom, it is possible to evaluate all the necessary cross sections in a self-consistent manner by the use of the experimental thermal-conductivity data provided that a knowledge of the viscosity, the internal specific heat capacity, and the internal relaxation number is available as a function of temperature in the limit of zero density. In principle, one can perform a similar analysis for more complicated molecules where there is a strong interaction between the rotational and the vibrational modes. In practice, such an analysis is hampered by insufficient knowledge of the behavior of the cross sections describing the diffusion of internal energy at high temperatures, which for rotating molecules provided valuable information. Furthermore, for the specific case of ethane, the lack of experimental data on rotational and vibrational collision numbers as a function of temperature makes the full analysis impossible to carry out. Nevertheless, a simplified form of the analysis was recently performed [13] and all the relevant cross sections were estimated. The analysis was based on a survey of all the available experimental thermal-conductivity data in the limit of zero density. As is customary [12, 13], a critical review was undertaken to establish the primary data set and ascertain the accuracy of the data. Subsequently the final representation of the thermal conductivity was generated. Since no new experimental measurements have been carried out since the earlier analysis, it was

decided to use the correlation in Ref. 13 unchanged for the present purpose of representing the thermal conductivity of ethane in the zero-density limit. Thus, a short recapitulation of the earlier correlation [13] is all that is necessary here.

From the results of the kinetic theory of dilute gases [9], one can express the thermal conductivity in terms of one effective collision cross section. In a practical, engineering form, the thermal conductivity in the zero density limit is given by

$$\lambda_0(T) = \frac{0.177568[T/M]^{1/2} C_P^0/R}{\sigma^2 \mathfrak{S}_\lambda^*} \tag{2}$$

where $\mathfrak{S}_\lambda^*$ is the reduced effective collision cross section, $T$ is the temperature in Kelvin, $M$ is the relative molecular mass, $\sigma$ is a length scaling parameter in nm, $C_P^0$ is the ideal isobaric molar heat capacity, $R$ is the gas constant, and $\lambda_0$ is in units of $\mathrm{mW \cdot m^{-1} \cdot K^{-1}}$. The numerical constant in Eq. (2) was obtained by the use of the most recent recommended values of the fundamental constants [45].

In developing the thermal-conductivity correlation, experimental values of $\mathfrak{S}_\lambda$ ($\mathfrak{S}_\lambda = \pi\sigma^2 \mathfrak{S}_\lambda^*$) were derived from each of the various primary data sources, which are listed in Ref. 13. Then the complete set of primary data for $\mathfrak{S}_\lambda^*(T^*)$ was fitted, by the use of appropriate statistical weights, to the functional form

$$\mathfrak{S}_\lambda^* = \sum_{i=0}^{n} a_i / T^{*i} \tag{3}$$

where the reduced temperature $T^*$ is given by

$$T^* = kT/\varepsilon \tag{4}$$

and $\varepsilon/k$ is the energy scaling parameter in Kelvin. In order to evaluate $\lambda_0$ from Eqs. (2)–(4), one needs a subsidiary representation for the molar heat capacity. For completeness, the ideal isobaric molar heat capacity of ethane is given by [13, 46]

$$C_P^0/R = f_8 + u \sum_{i=1}^{7} f_i X^{4-i} \tag{5}$$

$$u = \exp(-f_9 X) \tag{6}$$

$$X = T/100 \tag{7}$$

Table I contains all the relevant coefficients for the representation of the zero-density thermal conductivity and molar heat capacity of ethane.

**Table I.** Coefficients for the Representation of the Effective Collision Cross Section, Eq. (3), and the Heat Capacity, Eqs. (5)–(7), of Ethane[a]

| $i$ | $a_i$ | $f_i$ |
|---|---|---|
| 0 | 0.444 358 | — |
| 1 | 0.327 867 | 0.003 689 009 6 |
| 2 | 0.193 6835 | −0.171 969 07 |
| 3 | 0.0 | 3.159 226 |
| 4 | 0.0 | −8.045 994 2 |
| 5 | 0.0 | 7.423 767 3 |
| 6 | 0.0 | 0.0 |
| 7 | 0.0 | −2.072 457 2 |
| 8 | 0.0 | 4.0 |
| 9 | 0.0 | 0.02 |

[a] $\varepsilon/k = 264.70$ K; $\sigma = 0.43075$ nm; $M = 30.069$.

The resulting correlation [13] is valid in the temperature range 225 to 725 K, and its uncertainty is estimated to be $\pm 2.0\%$ in the range $300\ \text{K} \leqslant T \leqslant 500\ \text{K}$, increasing to $\pm 3.0\%$ at either end.

At high temperatures the available experimental evidence [47, 48], supported by a few numerical calculations and theoretical analysis [49], indicates that the Prandtl number of a dilute gas ($\text{Pr} = C_P^0 \eta_0 / M\lambda_0$) monotonically decreases to an almost-constant asymptotic value. The same behavior has been observed for ethane, indicating that the Prandtl number above 600 K can be taken as almost-constant, $\text{Pr} = 0.7$. This observation allows extension of the thermal-conductivity representation to its upper practical temperature limit of 1000 K. Hence, above $T = 725$ K the thermal conductivity of ethane in the zero-density limit can be estimated by means of

$$\lambda_0 = 11.877 \frac{\eta_0 C_P^0 / R}{M} \tag{8}$$

where $\eta_0$ is the viscosity in the zero-density limit in units of $\mu\text{Pa} \cdot \text{s}$ and is given in part I of this work [1], $C_P^0/R$ is given by Eqs. (5)–(7), and $M$ is the relative molecular mass given in Table I. The uncertainty of the correlation in this temperature range, $725\ \text{K} < T \leqslant 1000\ \text{K}$, is estimated to be $\pm 5.0\%$.

## 4. THE CRITICAL REGION

It has been observed for a number of pure fluids [7, 50–52] that the thermal conductivity shows a strong enhancement in a substantial region

around the critical point and becomes infinite at the critical point itself. According to the theory of dynamic critical phenomena [11] the enhancement of the thermal conductivity, $\Delta_c\lambda$, asymptotically close to the critical point can be related to the critical enhancement, $\Delta_c D_T$, of the thermal diffusivity by

$$\Delta_c\lambda = \rho C_P \Delta_c D_T \tag{9}$$

where $\rho$ is the density and $C_P$ is the specific heat at constant pressure. The critical enhancement of the thermal diffusivity has the following form asymptotically close to the critical point:

$$\Delta_c D_T = \frac{R_c k T}{6\pi\eta\xi} \tag{10}$$

where $\eta$ is the viscosity of the fluid, $\xi$ a correlation length, $k$ Boltzmann's constant, and $R_c$ a universal amplitude independent of the fluid. The asymptotic equations, (9) and (10), describe the transport properties only in an extremely small region around the critical point. In order to describe the critical enhancements of the transport properties in the larger range in which they are observed, we use crossover equations proposed by Olchowy and Sengers [53]. In their model they use the mode-coupling theory of dynamic critical phenomena [54] to generalize the asymptotic equation for the thermal conductivity to [53, 55]

$$\Delta_c\lambda = 7.5444 \times 10^{-4} \frac{T\rho C_P}{\eta\xi} (\Omega - \Omega_0) \tag{11}$$

where the temperature $T$ is in Kelvin, the viscosity $\eta$ in $\mu$Pa · s, the density $\rho$ in mol · L$^{-1}$, the specific heat capacity $C_P$ in J · mol$^{-1}$ · K$^{-1}$, the correlation length $\xi$ in nm, and the critical enhancement of the thermal conductivity $\Delta_c\lambda$ in mW · m$^{-1}$ · K$^{-1}$. The numerical constant in Eq. (11) was obtained by the use of the recommended values of fundamental constants [45] and the recommended value, 1.03, of the universal amplitude $R_c$ [56]. The remaining quantities $\Omega$ and $\Omega_0$ are crossover functions which depend on thermodynamic properties and on the background contributions to the thermal conductivity, $\bar{\lambda}$, and the viscosity, $\bar{\eta}$. They are presented in their most convenient form in Appendix II. The viscosity, $\eta$, in Eq. (11) is to be calculated from the equations presented in part I [1].

Hence, in order to evaluate the critical enhancement of the thermal conductivity by means of Eq. (11), one needs, apart from the background transport properties, a knowledge of three thermodynamic properties, namely, the isochoric and isobaric specific heat capacities and the correla-

tion length. The specific heat capacities can be evaluated directly from the relevant EOS, while the correlation length is related to the isothermal compressibility (susceptibility) of the fluid, which itself can be obtained from the EOS. For the sake of completeness we include the discussion on how, in practice, we calculate the correlation length.

Along the critical isochore ($\rho = \rho_c$), for temperatures above the critical temperature ($T \geqslant T_c$), the correlation length $\xi$ diverges according to

$$\xi = \xi_0(\Delta T)^{-\nu} \tag{12}$$

where $\Delta T = (T - T_c)/T_c$ is the reduced temperature difference, $\xi_0$ is a system-dependent amplitude, and $\nu$ is a universal critical exponent whose value is included in Table II. The dimensionless susceptibility of the fluid, defined as

$$\tilde{\chi} = \rho/(\partial\rho/\partial P)_T P_c \rho_c^{-2} \tag{13}$$

where $P_c$ is the critical pressure, also obeys a similar asymptotic power law,

$$\tilde{\chi} = \Gamma(\Delta T)^{-\gamma} \tag{14}$$

along the critical isochore. Here, $\gamma$ is another universal exponent, whose value is included in Table II, while the amplitude $\Gamma$ is system dependent.

**Table II.** Constants in the Equations for the Critical Thermal-Conductivity Enhancement

| | |
|---|---|
| **Critical parameters** | |
| $T_c$ | 305.33 K |
| $P_c$ | 4.8718 MPa |
| $\rho_c$ | 6.87 mol · L$^{-1}$ |
| **Critical exponents** | |
| $z$ | 0.063 |
| $\nu$ | 0.63 |
| $\gamma$ | 1.239 |
| **Critical amplitudes** | |
| $R$ | 1.03 |
| $\xi_0$ | 0.19 nm |
| $\Gamma$ | 0.0541 |
| **Cutoff wave number** | |
| $q_D^{-1}$ | 0.187 nm |

By eliminating the reduced temperature difference, $\Delta T$, from Eqs. (13) and (14), one obtains the following relationship along the critical isochore:

$$\xi = \xi_0(\tilde{\chi}/\Gamma)^{\nu/\gamma} \tag{15}$$

In practice, the above expression is generalized to hold for all temperatures and densities by writing [53]

$$\xi = \xi_0(\Delta_c\tilde{\chi}/\Gamma)^{\nu/\gamma} \tag{16}$$

where

$$\Delta_c\tilde{\chi} = \tilde{\chi}(T, \rho) - \tilde{\chi}(T_r, \rho)\frac{T_r}{T} \tag{17}$$

and $T_r$ is a reference temperature chosen sufficiently far above the critical temperature so that, for temperatures greater than $T_r$, the critical enhancement is negligible. We have determined the reference temperature by analysis of the thermal-conductivity data and adopted a value of $T_r = 1.5T_c$ as the most appropriate.

The remaining quantities to be determined in order to make use of Eqs. (11), (16), and (17) and those in Appendix II are the system-dependent amplitudes $\xi_0$ and $\Gamma$ and the cutoff wave number $q_D$. The former two values have been evaluated by application of the parametric crossover model to the EOS for ethane [14]. The numerical values of $\xi_0$ and $\Gamma$ are included in Table II. The cutoff wave number, $q_D$, has to be determined by fitting experimental data on the critical enhancement of the thermal conductivity to Eq. (11), and to make this possible a critical analysis of the available experimental data has to be undertaken in order to establish a consistent set of primary data.

There are several sets of thermal-conductivity data covering pressures and temperatures where the critical enhancement is observed. The most detailed work has been carried out by Mostert *et al.* [7, 43] along 11 isochores for a number of near-critical temperatures. The data were obtained with a parallel-plate method, which allows an approach to the critical point to within a few tenths of a degree. Mostert et al. [7] estimate that their experimental errors increase from $\pm 1\%$ somewhat away from the critical point to $\pm 5\%$ for data taken close to the critical point, and they state a spread of values of as much as $\pm 10\%$ for data on near-critical isochores within 0.4 K of the critical temperature. We took these figures as a guide upon which to base the uncertainty ascribed to their data. The other extensive set of data near the critical point has been obtained by Desmarest and Tufeu [42]. They reported measurements of the thermal conductivity of ethane along six isotherms in the extended critical region

obtained with a concentric-cylinder apparatus. No experimental uncertainty has been stated by the authors, so we based our estimates on previous measurements obtained with the same apparatus [57]. The uncertainty ascribed to this set of data is, on average, twice that of the data of Mostert et al. [7], and as is usual for data obtained in the critical region, the accuracy diminishes as the critical point is approached. Other sets of data [6, 32, 38, 40, 41] have been obtained in a much wider range of temperature and pressure, and the authors were not exclusively interested in the behavior of the thermal conductivity in the critical region. Nevertheless, some of the thermal-conductivity data they reported along a few isotherms exhibit a critical enhancement and were therefore included in the analysis. Three of the latter sets of data were obtained with a transient hot-wire method. Although this method is not suitable for measurements near the critical point, it was deemed that the measurements were carried out at temperatures and pressures far enough from the critical point that the data can be accepted provided that an appropriate increase is made in the uncertainty ascribed. All six sets of data have been taken as primary and are summarized in Table III, although one of the two 312 K isotherms in Refs. 40 and 41 had to be excluded because it was found to be inconsistent with the other data.

In order to analyze further these thermal-conductivity data and determine the cutoff wave number $q_D$, it is necessary first to separate the critical enhancement of the thermal conductivity from the other terms in Eq. (1). As described in part I and in our previous paper [12], it is difficult to perform the separation of the term $\Delta_c\lambda$ from the background term $\bar{\lambda}$ unequivocally, so an iterative approach has been applied. An initial estimate of the background thermal conductivity is made by the use of thermal-conductivity

**Table III.** Primary Experimental Data for the Critical Enhancement of the Thermal Conductivity of Ethane

| Reference | Method[a] | $T$(K) | $\rho$ (mol · L$^{-1}$) | Number of points |
|---|---|---|---|---|
| Millat et al. [6] | THW | 308, 331, 380, 426 | 0.2–4.3 | 28 |
| Mostert et al. [7, 43] | PP | 305–333 | 0.8, 2.5, 4.0, 5.3, 6.1, 6.9, 7.3, 8.00, 9.0, 10.5, 12.1 | 101 |
| Le Neindre et al. [32] | CC | 308, 343, 406 | 0.1–16.6 | 42 |
| Prasad & Venart [38] | THW | 295, 318, 350, 397 | 0.1–16.6 | 170 |
| Roder & Castro [40, 41] | THW | 295, 312, 325 | 0.1–16.6 | 420 |
| Desmarest & Tufeu [42] | CC | 309, 311, 315, 322, 335, 364 | 0.3–12.0 | 111 |

[a] CC, concentric cylinder; PP, parallel plate; THW, transient hot wire.

data for which the critical enhancement is negligible. This estimate is then used to evaluate the first iterate of $\Delta_c\lambda$ by subtracting the estimated background from data in the critical region. It is also used in the generation of $\Omega$ and $\Omega_0$ by means of the equations given in Appendix II, while $q_D$ is treated as an adjustable parameter in fitting $\Delta_c\lambda$. Once a first iterate value of $q_D$ is obtained, a refinement of the background contribution can be undertaken. In a subsequent iteration the whole set of thermal-conductivity primary data including the critical region is used to redetermine the background contribution by subtracting from each experimental thermal-conductivity value an appropriate critical enhancement calculated with the latest estimate of the parameter $q_D$. The new background is then used in equations given in Appendix II to redetermine the parameter $q_D$ by refitting the critical enhancement data to Eq. (11). The iterative process can then be continued until there is no significant change in either the background or the critical contributions. In practice, the process converges very rapidly, and for ethane only two iterations were necessary.

By means of the procedure described above, the critical enhancement of the thermal-conductivity, $\Delta_c\lambda$, term was evaluated from all of the primary experimental data given in Table III with the aid of Eq. (1). In this evaluation $\lambda_0$ for each isotherm was taken from the values reported by the individual authors if available. If unavailable, it was calculated from the correlation given by Eqs. (2)–(4).

The resulting data for $\Delta_c\lambda(\rho, T)$ were fitted to Eq. (11) by means of the auxiliary equations in Appendix II. The requisite thermodynamic quantities were estimated by the use of the appropriate EOS [5, 14]. In the fitting procedure a weight is assigned to each datum in accordance with the ascribed experimental uncertainty in the total thermal conductivity. All of the data in the critical region listed in Table III were found to be mutually consistent apart from the high-density, high-temperature data of Desmarest and Tufeu [42], which showed higher than expected deviations. There is no obvious reason why this should be so, and it would be difficult to justify excluding all the data from this region. Since the influence of these data on the determination of $q_D$ is small, it was decided to keep them in the primary data set but to increase their estimated uncertainty to $\pm 5\%$, thus decreasing their statistical weight.

Fitting all the primary data given in Table III we obtained an optimal value for the cutoff wave number of $q_D^{-1} = 0.187$ nm. This value is different from the value 0.17 nm obtained previously by Mostert et al. [7], who used a more local background thermal conductivity based on the analysis of fewer data and slightly different values for the amplitudes $\Gamma$ and $R_c$ and for the exponent $z$.

Figure 1 shows a comparison of the calculated thermal conductivity in

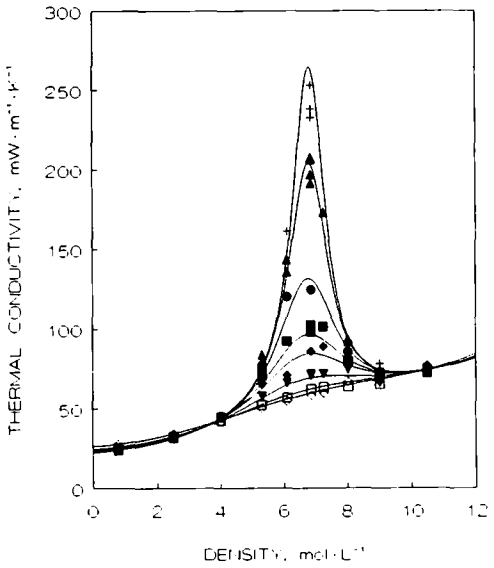


**Fig. 1.** The thermal conductivity as a function of density measured by Mostert et al. [7]: +, $T = 305.46$ K; ▲, $T = 305.56$ K; ●, $T = 306$ K; ■, $T = 307$ K; ◆, $T = 308$ K; ▼, $T = 312$ K; □, $T = 320$ K; ◇, $T = 333$ K. The solid lines represent the values calculated from Eq. (1).

the critical region with the data of Mostert *et al.* [7] along eight isotherms. The agreement is generally very good, and the deviations lie within the estimated error bounds, apart from a few points along the two isotherms nearest the critical isotherm, where deviations of as much as $\pm 15\%$ are observed. As pointed our earlier, the experimental scatter also increases under these conditions, mainly because of the increased uncertainty in the density, so that the agreement can be regarded as acceptable. Figure 2 shows a comparison with the data of Desmarest and Tufeu [42] along six isotherms. The agreement is still reasonably good at low densities and near-critical temperatures, but the deviations increase at higher densities and along isotherms farther away from the critical isotherm. Figure 3 contains a comparison with the data of Roder and Nieto de Castro [40, 41] and Prasad and Venart [38] in the vicinity of the critical point. Although some systematic trends can be observed, the agreement is still within the estimated uncertainty of these data in the critical region.

The final representation has also been used to predict the thermal diffusivity of ethane in the critical region by means of Eq. (10) so that the results can be compared with the thermal-diffusivity data of Jany and

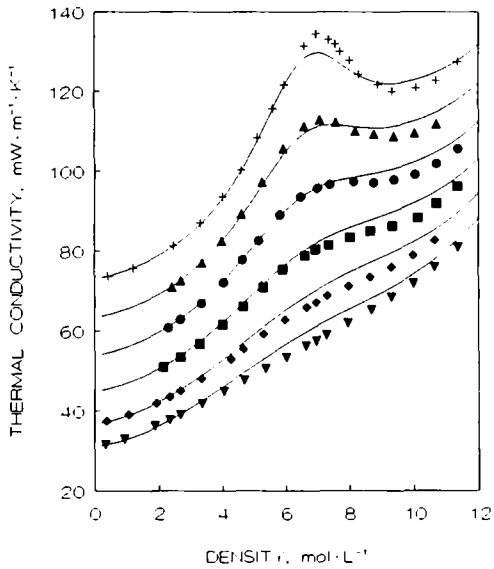


**Fig. 2.** The thermal conductivity as a function of density measured by Desmarest and Tufeu [42]: +, $T = 309$ K; ▲, $T = 311$ K; ●, $T = 315$ K; ■, $T = 322$ K; ◆, $T = 335$ K; ▼, $T = 364$ K. The solid lines represent the values calculated from Eq. (1). To separate the isotherms, the thermal-conductivity values have been displaced by 50, 40, 30, 20, 10, and 0 $mW \cdot m^{-1} \cdot K^{-1}$, respectively.

Straub [58] determined by a light-scattering technique along four near-critical isotherms. Since Jany and Straub [58] quote a value of 305.30 K for the critical temperature, $T_c$, rather than the value 305.33 K adopted in this paper, we compare experimental and calculated values at the same $\Delta T = T - T_c$ instead of at the same values of $T$. The agreement between the predicted thermal diffusivity and the measured one is very good as shown in Fig. A1 in Appendix III.

It should be emphasized that a critical enhancement of the thermal conductivity is present over a large range of densities and temperatures. Only outside the region bounded approximately by $225\ K \leqslant T \leqslant 457\ K$ and $0.3\ mol \cdot L^{-1} \leqslant \rho \leqslant 15.6\ mol \cdot L^{-1}$ is the relative critical thermal-conductivity enhancement, $\Delta_c \lambda / \lambda$, smaller than 1 %.

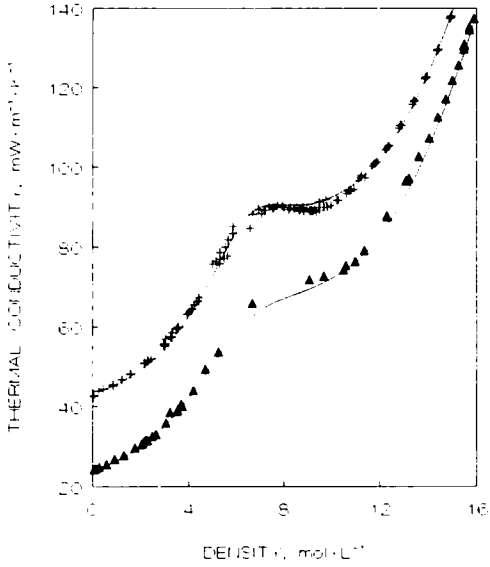


**Fig. 3.** The thermal conductivity as a function of density measured by Prasad and Venart [38] and Roder and Nieto de Castro [40, 41]: ▲, $T = 318$ K [38]; +, $T = 312$ K [40, 41]. The solid lines represent the values calculated from Eq. (1). To separate the isotherms, the thermal-conductivity values from Refs. 40 and 41 have been displaced by 20 mW · m$^{-1}$ · K$^{-1}$.

## 5. EXCESS THERMAL CONDUCTIVITY

The theoretical study of the thermal conductivity of a fluid as a function of density outside the critical region is not far advanced. In general, the existing models give only a qualitative picture and cannot be used to analyze the experimental data. Although at low densities greater theoretical advances have been made, it is not possible as yet to take advantage of these results when developing a correlation. Thus, unlike the viscosity [1], the analysis of the excess thermal conductivity is based entirely on experimental information. It has been customary [12, 15] to base the representation of the excess thermal conductivity on a power series expansion in density of the form

$$\Delta\lambda = \sum_{i=1}^{n} b_i \rho^i \tag{18}$$

where $b_i(T)$ are functions of temperature and are most conveniently represented in the following functional form

$$b_i = \sum_{j=0}^{m} e_{ij}/T^{*j} \tag{19}$$

where the reduced temperature is given by Eq. (4) and the units of coefficients $e_{ij}$ are $(\mathrm{L}\cdot\mathrm{mol}^{-1})^i$. These coefficients are obtained empirically by fitting the primary excess thermal-conductivity data, by use of the appropriate statistical weights, to Eqs. (18) and (19).

Before the fitting can be performed, the primary data set has to be established by analyzing all the available experimental data on the excess thermal conductivity of ethane. It is relatively straightforward to calculate the excess thermal conductivity, $\Delta\lambda$, from the experimental data, $\lambda$, by subtracting the zero density, $\lambda_0$, and the critical contribution, $\Delta_c\lambda$, according to Eq. (1). In practice, an iterative procedure is necessary, since the critical enhancement of the thermal conductivity can be calculated only if the background thermal conductivity is known. The scheme for separating the excess thermal conductivity from the critical enhancement of the thermal conductivity is described in detail in our previous work on carbon dioxide [12] and it was also summarized in Section 4 here. In the calculation of the excess thermal conductivity, through Eq. (1), in order to minimize systematic errors in the excess quantity, we have consistently used the zero-density values, $\lambda_0$, reported by the experimentalists. The critical enhancement of the thermal conductivity was calculated by means of Eq. (11).

There exist 15 sets of independent measurements [6, 7, 20, 21, 24, 27, 30–33, 36, 38–43] of the thermal conductivity of ethane at elevated pressures. Twelve sets of the measurements [6, 20, 21, 24, 27, 30–33, 36, 38–41] have been performed at conditions sufficiently far removed from the critical point such that the critical enhancement of the thermal conductivity is not a dominant contribution and can thus be used, in principle, to generate reliable excess thermal-conductivity values. Although the experimental data have been accumulated over 40 years, most of the measurements have been carried out in either concentric-cylinder or transient hot-wire instruments. Both of these two instruments, if used properly, can yield data of the highest accuracy and, as such, have to be considered as primary. Hence, the critical review of all the available data concentrated on the description of how the measurements were performed, on what corrections have been taken into account, and, more importantly, on consistency checks between different authors.

Initially, the consistency checks were carried out on seven sets of data [6, 20, 27, 31–33, 38, 40, 41], each of which covers a wide range of temperatures and pressures. These tests indicated that the data of Prasad

and Venart [38] and the data of Le Neindre et al. [31, 32], all of which cover mainly the supercritical region, are consistent within the estimated uncertainty. This finding was used as the basis for further comparisons with the data of other workers. The comparison has been performed along isotherms, a number of which happen to coincide among different experimentalists. Furthermore, if the data pertain to the supercritical region, one can compare the excess thermal conductivity along isotherms spaced apart by as much as $\pm 10$ K, since it has been observed for a number of supercritical fluids [15] that their excess transport properties are only very weakly temperature dependent.

Figure 4 shows the deviations of the excess thermal conductivity along the isotherm at 335 K for the data of five authors who have performed the measurements in its vicinity. In principle, the deviations can be taken with respect to any reasonable excess function since the purpose of the present discussion is to compare the data among themselves and establish a consistent set. In this work, in order to avoid unnecessary profusion of excess functions, all the deviations are taken from the final excess correlation. As illustrated in Fig. 4, the data of Millat et al. [6] and Rjabcev [33] broadly agree with the data of Le Neindre et al. [31, 32], while the data of Carmichael et al. [27] and Lenoir et al. [20] lie, on average, 7 and 4%, respectively, above them. Furthermore, the data of Lenoir et al. [20] show a large scatter, implying an excess thermal conductivity which is much more temperature dependent than the excess data of other authors. Thus,

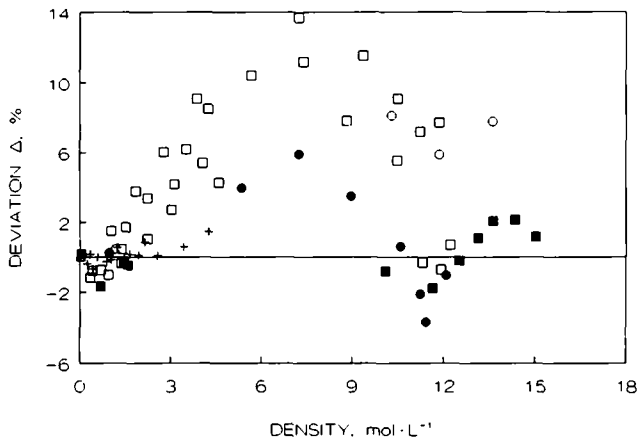


**Fig. 4.** Deviations, $\Delta$, from the final excess correlation, Eq. (18), of the excess thermal conductivity along a nominal 335 K isotherm: +, $T = 332$ K [6]; ●, $T = 343$ K [31, 32]; ■, $T = 331$ K [33]; ○, $T = 344$ K [27]; □, $T = 330$ and 340 K [20]. $\Delta = 100.0(\Delta\lambda_{exp} - \Delta\lambda_{cor})/\lambda_{cor}$.

the measurements of Carmichael et al. [27] and of Lenoir et al. [20] have been designated secondary. This choice is further strengthened a posteriori when one compares all the data of these two authors [20, 27] with the final representation (Fig. A4 in Appendix III).

Figures 5 and 6 compare the data of Millat et al. [6] and Rjabcev [33] along 410 and 480 K isotherms with the data of Prasad and Venart [38] and of Le Neindre et al. [31, 32]. The data of Millat et al. [6] are in good agreement with the data of Prasad and Venart [38] and of Le Neindre et al. [31, 32], while the data of Rjabcev [33] lie considerably lower. This is a surprising finding, since the data of Rjabcev [33] at supercritical temperatures below 380 K are in good agreement with the other results. By analyzing the data of Rjabcev in the vapor and liquid phases, further inconsistencies have been found with the results of other authors. No description of the apparatus of Rjabcev is available in the open literature, so it is very difficult to establish the reason for the discrepancies at low and high temperatures. This set has therefore also been classified as secondary. The remaining set of data encompasses the extensive measurements of Roder and Nieto de Castro [40, 41] including the liquid phase. The measurements have been performed in an apparatus with a proven record and the present data have been found consistent with the data of other authors [38]. Most of the data have been designated primary, except for 107 data points in the vicinity of the critical point, where the accuracy of the transient hot-wire technique rapidly diminishes.

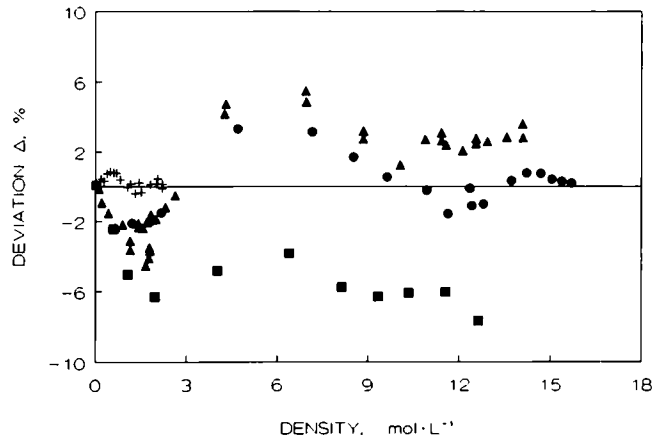


**Fig. 5.** Deviations, $\Delta$, from the final excess correlation, Eq. (18), of the excess thermal conductivity along a nominal 410 K isotherm: +, $T = 426$ K [6]; ▲, $T = 398$ K [38]; ●, $T = 406$ K [31, 32]; ■, $T = 418$ K [33]. $\Delta = 100.0(\Delta\lambda_{exp} - \Delta\lambda_{cor})/\lambda_{cor}$.

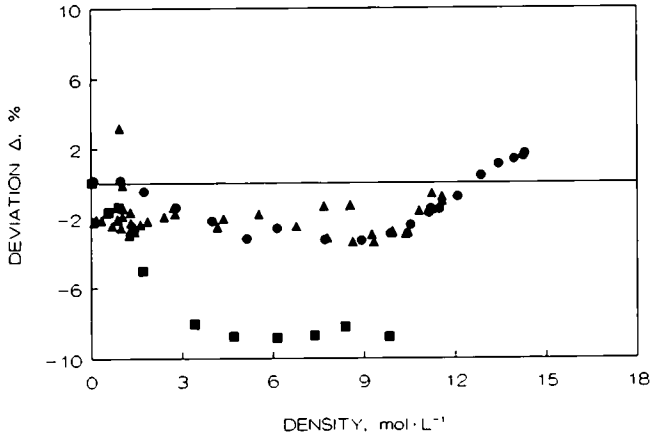


**Fig. 6.** Deviations, $\Delta$, from the final excess correlation, Eq. (18), of the excess thermal conductivity along a nominal 485 K isotherm: ▲, $T = 496$ K [38]; ●, $T = 483$ K [31, 32]; ■, $T = 478$ K [33]. $\Delta = 100.0(\Delta\lambda_{exp} - \Delta\lambda_{cor})/\lambda_{cor}$.

Rather than increase the estimated uncertainty, as has been illustrated in Section 4, these data points have been classified as secondary for the purpose of developing the excess thermal-conductivity representation.

The other five sets of data comprise measurements along one specific isotherm each. Only the measurements of Fleeter et al. [36] have been taken as primary on the basis of accuracy claimed and the method employed. Again, a posteriori examination of the other four sets of data

**Table IV.** Primary Experimental Data for the Excess Thermal Conductivity of Ethane

| Reference | Method[a] | $T$ (K) | $P$ (MPa) | Phase[b] | Number of points | Ascribed accuracy (%) |
|---|---|---|---|---|---|---|
| Le Neindre et al. [32] | CC | 308–800 | 0.1–119 | S | 113 | 3.0 |
| Fleeter et al. [36] | THW | 301 | 0.6–3.4 | V | 12 | 0.8 |
| Prasad & Venart [38] | THW | 293–296 | 0.2–3.8 | V | 16 | 3.0 |
| Prasad & Venart [38] | THW | 315–600 | 0.2–70 | S | 198 | 3.0 |
| Prasad & Venart [38] | THW | 294–297 | 4.5–70 | L | 25 | 3.0 |
| Roder & Castro [40, 41] | THW | 224–305 | 0.2–3.5 | V | 185 | 3.0 |
| Roder & Castro [40, 41] | THW | 306–328 | 0.1–68 | S | 270 | 3.0 |
| Roder & Castro [40, 41] | THW | 112–295 | 0.4–69 | L | 260 | 2.0 |
| Millat et al. [6] | THW | 308–426 | 0.5–6.6 | S | 64 | 0.8 |

[a] CC, concentric cylinder, THW, transient hot wire.
[b] V, vapor; L, liquid; S, supercritical.

**Table V.** Coefficients for the Representation of the Excess Thermal Conductivity of Ethane, Eqs. (18) and (19): $\Delta\lambda = \sum_{i=1}^{6} \sum_{j=0}^{2} e_{ij} \rho^i / T^{*j}$

| $i$ | $e_{i0}$ | $e_{i1}$ | $e_{i2}$ |
|---|---|---|---|
| 1 | 1.179 5365 | −1.532 0900 | 2.015 9682 |
| 2 | 3.118 8977 | −4.716 6037 | 0.0 |
| 3 | $-8.357\,2937 \times 10^{-1}$ | 1.457 5942 | 0.0 |
| 4 | $8.572\,9762 \times 10^{-2}$ | $-1.635\,4312 \times 10^{-1}$ | 0.0 |
| 5 | $-3.575\,1570 \times 10^{-3}$ | $7.930\,1012 \times 10^{-3}$ | $-1.649\,6369 \times 10^{-4}$ |
| 6 | $4.962\,6960 \times 10^{-5}$ | $-1.365\,2796 \times 10^{-4}$ | $6.605\,2581 \times 10^{-6}$ |

[21, 24, 30, 39], displayed together with the data in Refs. 20 and 27, in Fig. A4, in Appendix III, indicates that, in general, these later data deviate considerably from the final representation and could not have been taken as primary.

Table IV lists all the experimental data chosen as primary for the purpose of developing the representation of the excess thermal conductivity. The estimated uncertainty in each data set is also given. The estimate is based upon our modification of the uncertainty claimed by the original authors either as a result of checks of consistency or as a result of an

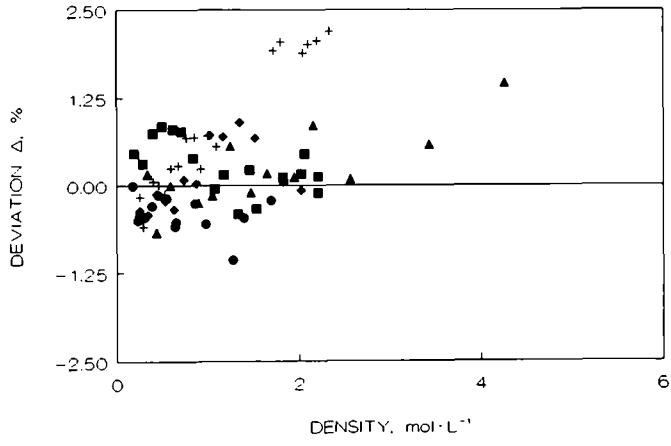


**Fig. 7.** Deviations, $\Delta$, from the final excess correlation, Eq. (18), of the excess thermal conductivity deduced from data of Millat et al. [6] and Fleeter et al. [36]: +, $T = 308$ K [6]; ▲, $T = 332$ K [6]; ●, $T = 380$ K [6]; ■, $T = 425$ K [6]; ◆, $T = 301$ K [36]. $\Delta = 100.0(\Delta\lambda_{exp} - \Delta\lambda_{cor})/\lambda_{cor}$.

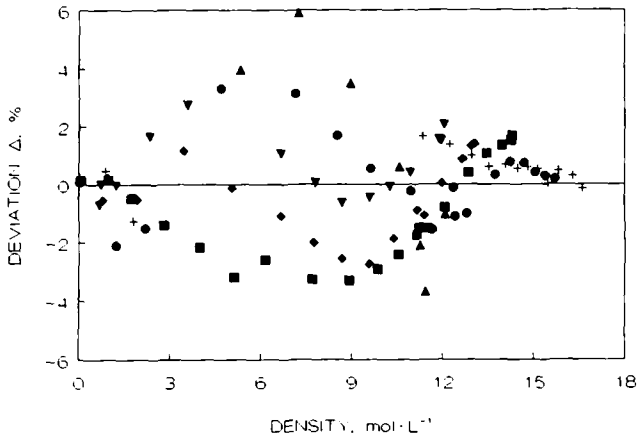


**Fig. 8.** Deviations, $\Delta$, from the final excess correlation, Eq. (18), of the excess thermal conductivity deduced from data of Le Neindre et al. [31, 32]: +, $T = 308$ K; ▲, $T = 343$ K; ●, $T = 406$ K; ■, $T = 483$ K; ◆, $T = 571$ K; ▼, $T = 649$ K. $\Delta = 100.0(\Delta\lambda_{exp} - \Delta\lambda_{cor})/\lambda_{cor}$.

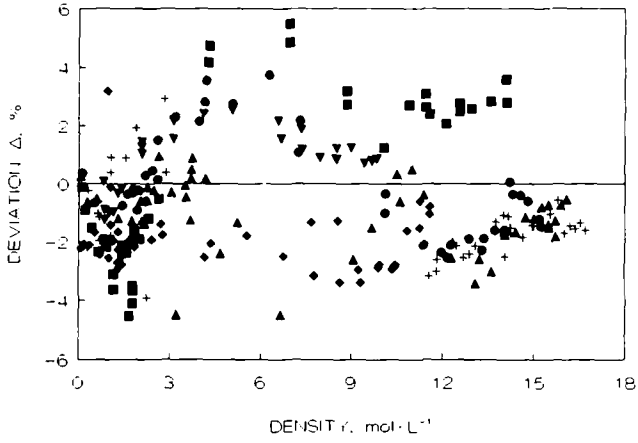


**Fig. 9.** Deviations, $\Delta$, from the final excess correlation, Eq. (18), of the excess thermal conductivity deduced from data of Prasad and Venart [38]: +, $T = 293$–$296$ K; ▲, $T = 314$–$319$ K; ●, $T = 348$–$351$ K; ■, $T = 394$–$399$ K; ◆, $T = 495$–$598$ K; ▼, $T = 598$–$600$ K. $\Delta = 100.0(\Delta\lambda_{exp} - \Delta\lambda_{cor})/\lambda_{cor}$.

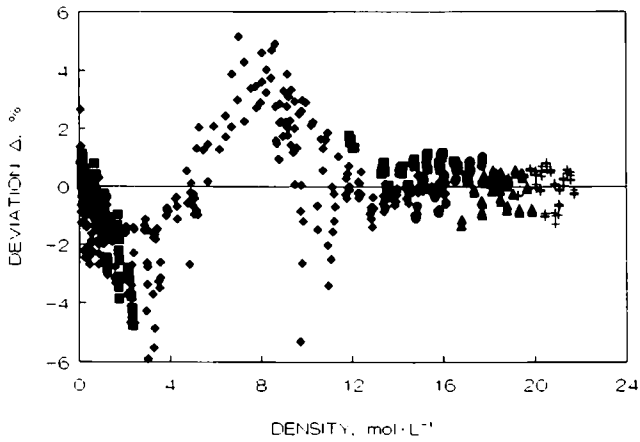


**Fig. 10.** Deviations, $\Delta$, from the final excess correlation, Eq. (18), of the excess thermal conductivity deduced from data of Roder and Nieto de Castro [40, 41]: +, $T = 111$–$156$ K; ▲, $T = 174$–$216$ K; ●, $T = 224$–$266$ K; ■, $T = 273$–$296$ K; ◆, $T = 303$–$326$ K. $\Delta = 100.0(\Delta\lambda_{exp} - \Delta\lambda_{cor})/\lambda_{cor}$.

examination of their earlier work for other fluids. Although, the primary data set encompasses a temperature range $122\ \text{K} \leqslant T \leqslant 800\ \text{K}$, the EOS [5] available is valid only up to 625 K. Thus, it was not possible to analyze or include in the present correlation 20 experimental measurements of the thermal conductivity [32] that are available at temperatures above 625 K.

By means of the procedure described in part I, all the primary data were fitted to Eqs. (18) and (19) by the use of the stepwise least-squares SEEQ algorithm [59]. The optimal values of coefficients $e_{ij}$ are given in Table V. Figures 7–10 display the deviations of the primary excess experimental data for the thermal conductivity of ethane from the representation developed here. Figures 8 and 9 show superficial indications of deviations of the data of Prasad and Venart [38] and of Le Neindre et al. [31, 32] from the final representation. However, the accuracy of the data in this region is no better than $\pm 2$–$3\%$ so that the trends are, strictly, insignificant. Furthermore, the deviations are no greater than the accuracy claimed for the representation of the thermal conductivity ($\pm 4\%$) in the relevant part of the phase space.

## 6. THE OVERALL REPRESENTATION

The final representation of the thermal conductivity of ethane is given by Eq. (1). The zero-density term, $\lambda_0$, is given by Eqs. (2)–(7) with the

coefficients in Table I. The excess thermal conductivity, $\Delta\lambda$, is given by Eqs. (18) and (19) with the coefficients in Table V. The critical enhancement term, $\Delta_c\lambda$, is given by Eq. (11) with the coefficients in Table II and the auxiliary equations defined in Appendix II. Appendix III contains a number of figures showing the deviations of the experimental thermal-conductivity data from those obtained on the basis of the present correlation for the selected sets of data. Only primary data in the vapor and supercritical phase are shown in Fig. A2, since the final deviation plot for the liquid primary data is essentially the same as that in Fig. 10.

Figure 11 illustrates the range of applicability of the present representation as well as the estimated uncertainty in various thermodynamic regions. The correlation can be used up to 625 K and 70 MPa. Any extrapolation to higher temperatures or pressures can lead to a rapid reduction in the accuracy of the predicted thermal conductivity and is not recommended, although at very low pressures, below 10 bar, Eq. (1) can be used to predict the thermal conductivity up to 1000 K. The lower temperature limit in the gaseous phase is 225 K, while the overall correlation can be used to estimate the liquid phase thermal conductivity down to 100 K.

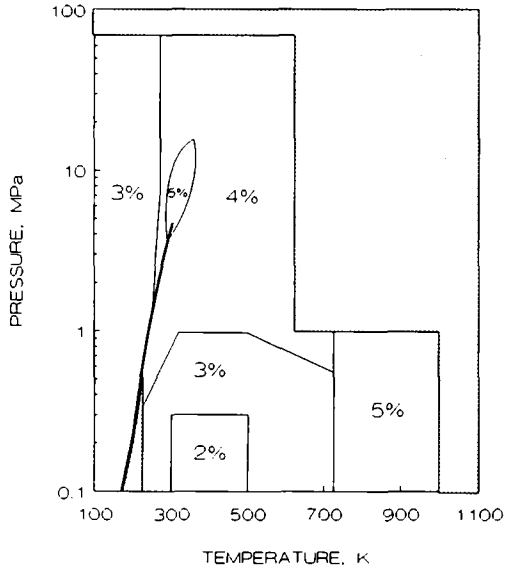


**Fig. 11.** The extent of the thermal-conductivity representation and its estimated uncertainty. No representation is available in the hatched region.

In Appendix IV (Table AII) the thermal conductivity of ethane along a number of isotherms as a function of pressure is tabulated. Appendix V (Table AIII) contains the values of the thermal conductivity along the saturation line. The values of the thermal conductivity in both appendices were generated directly from the representation given here. The values of the thermal conductivity as a function of temperature and density given in Appendix V can, in addition, be used to assist those programming the representative equations with checking of their coding.

## 7. DISCUSSION

It is interesting to compare the new representation with those developed earlier to ascertain if the inclusion of new experimental data sets or a different approach in representing the data leads to substantial differences. Although a number of correlations have been proposed for the thermal conductivity of ethane [2–5] in the past, an extensive comparison has been made only with that most recently published [5], which has, to all intents and purposes, superseded all the older ones both in extent and in claimed accuracy. Figure 12 shows the deviations between the two representations along a number of selected isotherms. The isotherms have been specifically chosen to be representative of the behavior in the thermodynamic regions

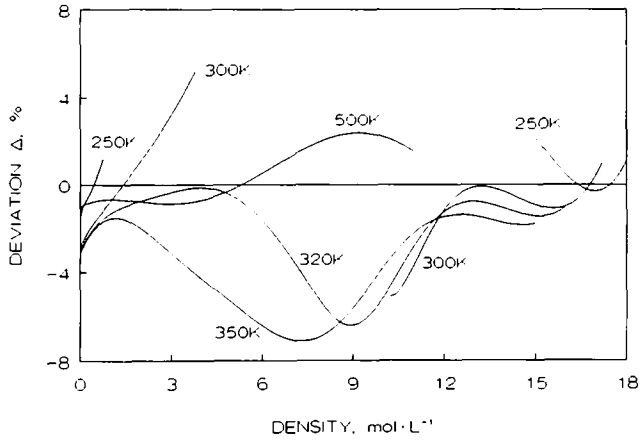


**Fig. 12.** Deviations, $\Delta$, from the final correlation, Eq. (1), of the thermal conductivity evaluated by the use of the Friend et al. correlation [5]. $\Delta = 100.0(\Delta\lambda_{FIE} - \Delta\lambda_{cor})/\lambda_{cor}$.

where the two correlations differ in their approach to the development of the representation.

The deviations at zero density between the two correlations seem to be largest around room temperature, leading to differences of $\pm 3\%$. Although these deviations are within the combined uncertainty ascribed to the correlations, we believe that at low densities the present representation is an improvement on the previous one not only because it includes recently published data of Millat *et al.* [6], but also because it is based on a sound theoretical foundation. In the remainder of the vapor phase, deviations seem to increase as one approaches the saturation curve.

In the supercritical region, where the contribution of the critical enhancement is appreciable, large deviations between the two correlations are observed as is illustrated by isotherms 320 and 350 K in Fig. 12. In some density regions the correlation in Ref. 5 underestimates the thermal conductivity by as much as 8%. It is important to stress that these differences are observed at temperatures 15–60 K away from the critical temperature. In the vicinity of the critical point much larger differences between the two correlations are observed. Some of this behavior is simply a result of the fact that the thermal conductivity is a strong function of density in this region. The differences illustrated in Fig. 12 for the 320 and 350 K isotherms can be attributed to the inclusion of new experimental

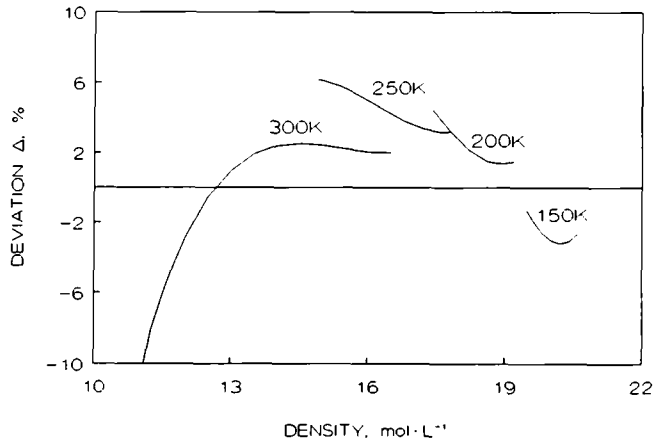


**Fig. 13.** Deviations, $\Delta$, from the final correlation, Eq. (1), of the thermal conductivity evaluated by the use of the Assael et al. [60] hard-sphere prediction scheme. $\Delta = 100.0(\lambda_{HS} - \lambda_{cor})/\lambda_{cor}$.

data [7] in this region and to applications of the full theory of the critical enhancement in the present work. Thus, again we believe that the present representation in the critical region is an improvement on the previous one [5]. At temperatures very far from the critical temperature the deviations are within the estimated uncertainty of the two correlations and are of the order of $\pm 2$–3%.

In the liquid phase both correlations are based on the same experimental data and the deviations are, in general, small. Nevertheless, as the saturation line is approached, larger differences are observed, which again can be attributed to the treatment of the critical enhancement.

In developing the thermal-conductivity representation no theoretical guidance was used for the behavior of thermal conductivity in the liquid phase. In line with our previous analysis of the liquid viscosity of ethane, described in part I [1], we compare the results of our correlation with the predictions of the scheme developed by Assael et al. [60]. Since the analogous scheme for viscosity is briefly summarized in part I [1], it is sufficient to note that the scheme developed for the thermal conductivity is also based on hard-sphere theory and that it is claimed to be possible to predict the thermal conductivity of a particular liquid at a prescribed temperature and density with an estimated accuracy of $\pm 6\%$.

Figure 13 shows the deviations of the predicted thermal conductivity from the values obtained by the use of the present representation along four liquid-phase isotherms. The deviations are within the accuracy claimed by Assael et al. [60] in most of the liquid phase. The exception is the region near the liquid saturation density at temperatures just below the critical, where the critical enhancement becomes increasingly important. Since the scheme of Assael et al. [60] does not take critical phenomena into account, its failure in this region of the phase space is not surprising.

## 8. CONCLUSION

The representation of the thermal conductivity of ethane encompassing a large region of thermodynamic states has been presented. The formulation is based on a critical analysis of experimentally available data guided by theoretical results. The uncertainty ascribed to the thermal conductivity is nowhere greater than $\pm 5\%$, which, for many engineering purposes, will prove adequate. Nevertheless, it would be advantageous to have more accurate measurements, especially in the vapor phase, where the uncertainties in the thermal conductivity are larger than for other gases studied.

## APPENDIX I

**Table AI.** List of All the Available Data from Measurements of the Thermal Conductivity of Ethane

| Ref. No. | Method[a] | $T$(K) | $P$(MPa) | Phase[b] |
|---|---|---|---|---|
| 16 | SSHW | 202–273 | 0.1 | ZD |
| 17 | SSHW | 273–293 | 0.1 | ZD |
| 18 | CC | 343 | 0.1 | ZD |
| 19 | CC | 303 | 0.1 | ZD |
| 20 | CC | 315–340 | 0.1–19.8 | ZD, S |
| 21 | CC | 325 | 1.0–4.0 | ZD, S |
| 22 | SSHW | 374–399 | 0.1 | ZD |
| 23 | SSHW | 339 | 0.1 | ZD |
| 24 | CC | 341 | 0.1–26 | ZD, S |
| 25 | SSHW | 272–873 | 0.1 | ZD |
| 26 | CC | 273–673 | 0.1 | ZD |
| 27 | SCC | 278–444 | 0.1–36.6 | ZD, V, L, S |
| 28 | NK | 303 | 0.1 | ZD |
| 29 | SSHW | 275–864 | 0.1 | ZD |
| 30 | CC | 348 | 0.1–304 | ZD, S |
| 31, 32 | CC | 308–800 | 0.1–119 | ZD, S |
| 33 | NK | 191–572 | 0.1–53.4 | ZD, V, L, S |
| 34 | THW | 303 | 0.1 | ZD |
| 35 | HF | 318–590 | 0.1 | ZD |
| 36 | THW | 301 | 0.6–3.4 | ZD, V |
| 37 | CC | 307–500 | — | ZD, S |
| 38 | THW | 293–600 | 0.2–70 | ZD, V, L, S |
| 39 | CC | 299 | 0.1–11.8 | ZD, V, L |
| 40, 41 | THW | 112–328 | 0.1–69 | ZD, V, L, S |
| 42 | CC | 309–365 | 1.0–28.2 | ZD, S |
| 6 | THW | 308–426 | 0.5–6.6 | ZD, S |
| 7, 43 | PP | 305–333 | 1.9–18.3 | S |

[a] CC, concentric cylinder; SCC, spherical conductivity cell; SSHW, steady-state hot wire; THW, transient hot wire; PP, parallel plate; HF, heated filament; NK, not known.
[b] ZD, zero density; V, vapor; L, liquid; S, supercritical.

## APPENDIX II

**Expressions for the Crossover Functions $\Omega$ and $\Omega_0$ Entering the Description of the Critical Enhancement of the Thermal Conductivity, Eq. (11)**

$$\Omega(\{y_i\}) = \frac{2}{\pi}\frac{1}{(1+y_\gamma)}\left\{y_D - F(z_i, y_D)\sum_{i=1}^{4}\frac{(a_3 z_i^3 + a_2 z_i^2 + a_1 z_i + a_0)}{\sum_{j=1, j\neq i}^{4}(z_i - z_j)}\right\} \tag{A1}$$

$$\Omega_0 = \frac{1 - \exp\{-[(q_D\xi)^{-1} + (q_D\xi\rho_c/\rho)^2/3]^{-1}\}}{(\pi/2)[1 + y_\alpha(y_D + y_\delta) + y_\beta/(1+y_\gamma)]} \tag{A2}$$

$$\prod_{i=1}^{4}(z + z_i) = z^4 + b_3 z^3 + b_2 z^2 + b_1 z + b_0 = 0 \tag{A3}$$

$$\begin{aligned} a_0 &= y_\gamma^2 - y_\alpha y_\gamma y_\delta \\ a_1 &= y_\alpha y_\gamma y_D \\ a_2 &= y_\gamma - y_\beta - y_\alpha y_\delta \\ a_3 &= y_\alpha y_D \end{aligned} \tag{A4}$$

$$\begin{aligned} b_0 &= y_\alpha y_\gamma y_\delta \\ b_1 &= y_\alpha y_\gamma y_D \\ b_2 &= y_\gamma + y_\beta + y_\alpha y_\delta \\ b_3 &= y_\alpha y_D \end{aligned} \tag{A5}$$

Auxiliary functions

$$F(x, y_D) = \frac{1}{(1-x^2)^{1/2}}\ln\left[\frac{1 + x + (1-x^2)^{1/2}\,\mathrm{tg}(y_D/2)}{1 + x - (1-x^2)^{1/2}\,\mathrm{tg}(y_D/2)}\right] \tag{A6}$$

$$y_D = \mathrm{arctg}(q_D\xi) \tag{A7}$$

$$y_\delta = \frac{\mathrm{arctg}[q_D\xi/(1 + q_D^2\xi^2)^{1/2}] - y_D}{(1 + q_D^2\xi^2)^{1/2}} \tag{A8}$$

$$y_\gamma = C_V/(C_P - C_V) \tag{A9}$$

$$y_\alpha = 5.4935 \times 10^{-4}\frac{M\rho T}{\xi\bar{\eta}^2} \tag{A10}$$

$$y_\beta = \frac{M\bar{\lambda}}{(C_P - C_V)\bar{\eta}} \tag{A11}$$

where $T$ is the temperature in Kelvin, $\rho$ is the density in $\text{mol} \cdot \text{L}^{-1}$, $M$ is the relative molecular mass, $\bar{\eta}$ is the background viscosity in $\mu\text{Pa} \cdot \text{s}$, $\bar{\lambda}$ is the background thermal conductivity in $\text{mW} \cdot \text{m}^{-1} \cdot \text{K}^{-1}$, $C_P$ and $C_V$ are isobaric and isochoric heat capacities, respectively, in $\text{J} \cdot \text{mol}^{-1} \cdot \text{K}^{-1}$, $\xi$ is a correlation length in nm, and $q_D$ is a large wave-number cutoff parameter in $\text{nm}^{-1}$.

The thermodynamic functions $C_P$, $C_V$, and $\xi$, which is related to the compressibility through Eq. (16), are calculated from the EOS as specified in Section 2. The background thermal conductivity, $\bar{\lambda}$, is given by

$$\bar{\lambda}(\rho, T) = \lambda_0(T) + \Delta\lambda(\rho, T) \tag{A12}$$

with $\lambda_0(T)$ calculated from Eq. (2) and $\Delta\lambda(\rho, T)$ from Eq. (18). The background viscosity, $\bar{\eta}$, is given by

$$\bar{\eta}(\rho, T) = \eta_0(T) + \Delta\eta(\rho, T) \tag{A13}$$

with the dilute-gas viscosity, $\eta_0(T)$, and the excess viscosity, $\Delta\eta(\rho, T)$, to be calculated as specified in part I [1].

# APPENDIX III

## Deviation Plots of the Selected Experimental Data from the Correlation

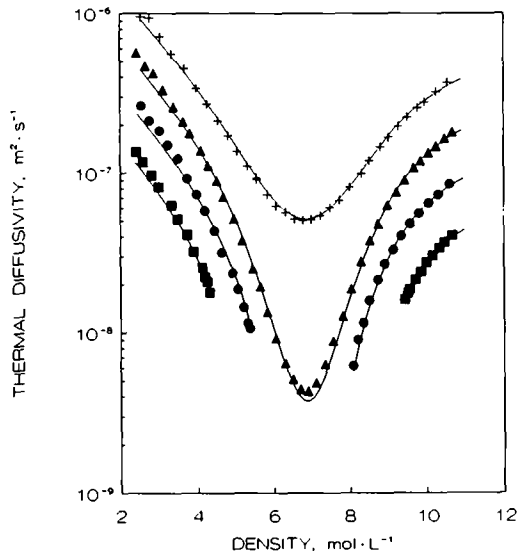


**Fig. A1.** The thermal diffusivity as a function of density measured by Jany and Straub [58]: ■, $T = 302.28$ K; ●, $T = 305.02$ K; ▲, $T = 305.64$ K; +, $T = 308.38$ K. The solid lines represent the values calculated from Eq. (10). To separate the isotherms the thermal-diffusivity values have been multiplied by 1, 2, 4, and 8, respectively.

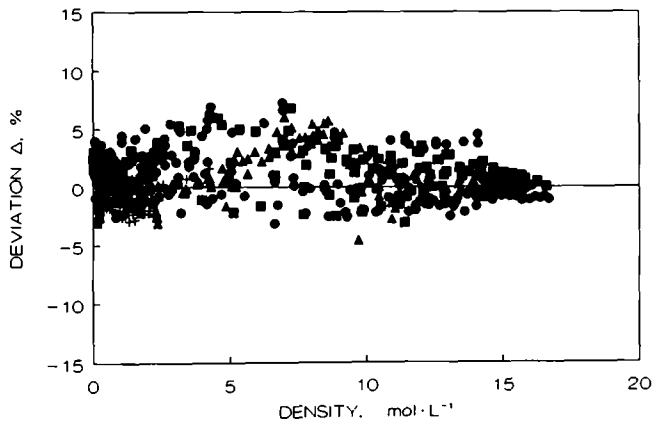


**Fig. A2.** Deviations, $\Delta$, from the final correlation, Eq. (1), of the primary thermal-conductivity data in the vapor and supercritical regions: + [6]; ▲ [40, 41]; ● [38]; ■ [31, 32]. $\Delta = 100.0(\lambda_{exp} - \lambda_{cor})/\lambda_{cor}$.

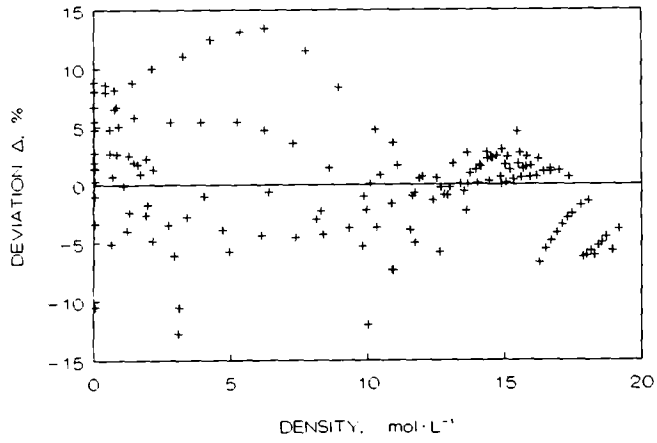


**Fig. A3.** Deviations, $\Delta$, from the final correlation, Eq. (1), of the secondary thermal-conductivity data of Rjabcev [33]. $\Delta = 100.0(\lambda_{exp} - \lambda_{cor})/\lambda_{cor}$.

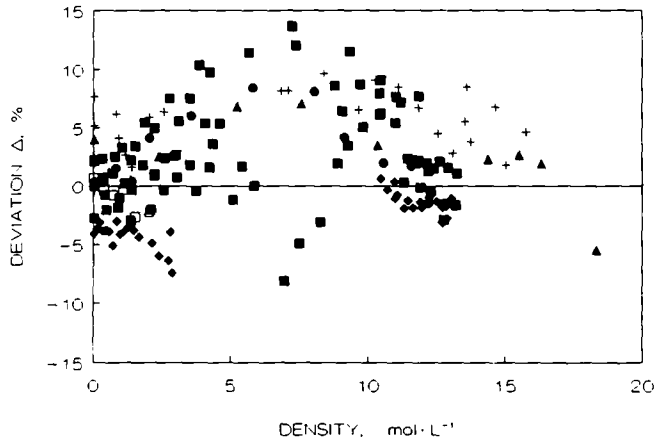


**Fig. A4.** Deviations, $\Delta$, from the final correlation, Eq. (1), of the selected secondary thermal-conductivity data: + [27]; ▲ [30]; ● [24]; ■ [20]; ◆ [39]; □ [21]. $\Delta = 100.0(\lambda_{exp} - \lambda_{cor})/\lambda_{cor}$.

140 15 1-5

## APPENDIX IV

**Table AII.** Tabulation of the Thermal Conductivity of Ethane

| | Thermal conductivity of ethane, $\lambda$ ($mW \cdot m^{-1} \cdot K^{-1}$), at $T$(K) | | | | | | | | | | | |
|---|---|---|---|---|---|---|---|---|---|---|---|---|
| $P$(MPa) | 100 | 150 | 200 | 250 | 275 | 300 | 306 | 310 | 350 | 400 | 500 | 600 |
| 0.10 | 239.94 | 202.12 | — | 15.58 | 18.57 | 21.81 | 22.63 | 23.18 | 28.98 | 36.89 | 54.35 | 73.15 |
| 0.50 | 240.23 | 202.45 | 151.09 | 16.09 | 18.95 | 22.10 | 22.90 | 23.44 | 29.16 | 37.03 | 54.45 | 73.23 |
| 1.00 | 240.59 | 202.86 | 151.65 | 16.96 | 19.57 | 22.57 | 23.34 | 23.86 | 29.44 | 37.23 | 54.59 | 73.35 |
| 2.00 | 241.31 | 203.68 | 152.77 | 107.91 | 21.57 | 23.95 | 24.62 | 25.09 | 30.24 | 37.73 | 54.93 | 73.65 |
| 3.00 | 242.02 | 204.49 | 153.87 | 109.51 | 89.63 | 26.39 | 26.78 | 27.10 | 31.44 | 38.43 | 55.35 | 74.02 |
| 5.00 | 243.43 | 206.08 | 156.01 | 112.55 | 93.61 | 76.09 | 76.81 | 44.47 | 35.66 | 40.56 | 56.40 | 74.94 |
| 8.00 | 245.48 | 208.40 | 159.11 | 116.79 | 98.84 | 82.79 | 79.27 | 77.00 | 49.96 | 46.11 | 58.46 | 76.67 |
| 10.00 | 246.82 | 209.90 | 161.10 | 119.45 | 102.00 | 86.64 | 83.29 | 81.14 | 61.68 | 51.18 | 60.09 | 77.98 |
| 20.00 | 253.09 | 216.86 | 170.26 | 131.21 | 115.33 | 101.80 | 98.89 | 97.03 | 81.78 | 71.22 | 69.13 | 84.70 |
| 30.00 | 258.71 | 223.02 | 178.31 | 141.17 | 126.21 | 113.54 | 110.82 | 109.08 | 94.56 | 83.32 | 77.39 | 90.26 |
| 40.00 | 263.74 | 228.45 | 185.39 | 149.84 | 135.55 | 123.45 | 120.86 | 119.19 | 105.16 | 93.64 | 85.18 | 95.08 |
| 50.00 | 268.19 | 233.23 | 191.68 | 157.50 | 143.75 | 132.11 | 129.61 | 128.00 | 114.37 | 102.80 | 92.77 | 99.91 |
| 70.00 | 275.50 | 240.98 | 202.40 | 170.44 | 157.59 | 146.67 | 144.32 | 142.81 | 129.89 | 118.54 | 107.09 | 110.16 |

## APPENDIX V

**Table AIII.** Thermal Conductivity of Ethane Along the Saturation Line

| $T$ (K) | $P$ (MPa) | $\rho_{vap.}$ (mol·L$^{-1}$) | $\lambda_{vap.}$ (mW·m$^{-1}$·K$^{-1}$) | $\rho_{liq.}$ (mol·L$^{-1}$) | $\lambda_{liq.}$ (mW·m$^{-1}$·K$^{-1}$) |
|---|---|---|---|---|---|
| 100.0 | $1.1 \times 10^{-5}$ | $1.3 \times 10^{-5}$ | — | 21.323 | 239.76 |
| 120.0 | $3.55 \times 10^{-4}$ | $3.56 \times 10^{-4}$ | — | 20.597 | 229.69 |
| 140.0 | $3.83 \times 10^{-3}$ | $3.30 \times 10^{-3}$ | — | 19.852 | 212.15 |
| 160.0 | 0.02145 | 0.01631 | — | 19.081 | 191.55 |
| 180.0 | 0.07872 | 0.05412 | — | 18.276 | 170.75 |
| 200.0 | 0.2174 | 0.1387 | — | 17.423 | 150.71 |
| 220.0 | 0.4923 | 0.3001 | — | 16.498 | 132.00 |
| 230.0 | 0.7005 | 0.4221 | 14.49 | 15.999 | 123.21 |
| 240.0 | 0.9671 | 0.5810 | 16.00 | 15.467 | 114.78 |
| 250.0 | 1.3012 | 0.7867 | 17.70 | 14.892 | 106.73 |
| 260.0 | 1.7120 | 1.0534 | 19.70 | 14.261 | 99.07 |
| 270.0 | 2.2097 | 1.4038 | 22.19 | 13.551 | 91.82 |
| 280.0 | 2.8058 | 1.8787 | 25.59 | 12.723 | 85.14 |
| 290.0 | 3.5144 | 2.5703 | 31.07 | 11.683 | 79.39 |
| 295.0 | 3.9169 | 3.0723 | 35.78 | 11.010 | 76.97 |
| 300.0 | 4.3560 | 3.8129 | 44.68 | 10.101 | 75.12 |
| 302.0 | 4.5432 | 4.2616 | 52.00 | 9.5867 | 75.30 |
| 304.0 | 4.7377 | 4.9547 | 71.97 | 8.8412 | 79.81 |

## ACKNOWLEDGMENTS

Financial support for the IUPAC Transport Properties Project Centre at Imperial College is provided by the U.K. Department of Trade and Industry. The research at the University of Maryland is supported by the Division of Chemical Sciences of the Office of Basic Energy Sciences of the U.S. Department of Energy under Grant DE-FG05-88ER-13902. The collaboration between Imperial College and University of Maryland is supported by NATO Research Grant 0008/88, the collaboration with the Universities of Rostock and Thessaloniki is supported by the British Council and Deutscher Akademischer Austauschdienst, and that between the University of Rostock and the University of Thessaloniki was part of the Greek–German Agreement on Scientific Cooperation. This work was carried out under the auspices of the Subcommittee on Transport Properties of Commission I.2 of the International Union of Pure and Applied Chemistry.

## REFERENCES


1. S. Hendl, J. Millat, E. Vogel, V. Vesovic, W. A. Wakeham, J. Luettmer-Strathmann, J. V. Sengers, and M. J. Assael, *Int. J. Thermophys.* **15**:1 (1994).
2. N. B. Vargaftik, *Tables of the Thermophysical Properties of Liquids and Gases* (Halsted Press, New York, 1975).
3. H. J. M. Hanley, K. E. Gubbins, and S. Murad, *J. Phys. Chem. Ref. Data* **6**:1167 (1977).
4. B. A. Younglove and J. F. Ely, *J. Phys. Chem. Ref. Data* **16**:577 (1987).
5. D. G. Friend, H. Ingham, and J. F. Ely, *J. Phys. Chem. Ref. Data* **20**:275 (1991).
6. J. Millat, M. Ross, W. A. Wakeham, and M. Zalaf, *Int. J. Thermophys.* **9**:481 (1988).
7. R. Mostert, H. R. van den Berg, P. S. van der Gulik, and J. V. Sengers, *J. Chem. Phys.* **92**:5454 (1990).
8. G. C. Maitland, M. Rigby, E. B. Smith, and W. A. Wakeham, *Intermolecular Forces: Their Origin and Determination* (Clarendon Press, Oxford, 1987).
9. F. R. W. McCourt, J. J. M. Beenakker, W. E. Kohler, and I. Kuscer, *Non-Equilibrium Phenomena in Polyatomic Gases* (Clarendon Press, Oxford, 1991).
10. J. Millat, V. Vesovic, and W. A. Wakeham, *Int. J. Thermophys.* **10**:805 (1989).
11. J. V. Sengers, *Int. J. Thermophys.* **6**:203 (1985).
12. V. Vesovic, W. A. Wakeham, G. A. Olchowy, J. V. Sengers, J. T. R. Watson, and J. Millat, *J. Phys. Chem. Ref. Data* **19**:763 (1990).
13. S. Hendl, J. Millat, V. Vesovic, E. Vogel, and W. A. Wakeham, *Int. J. Thermophys.* **12**:999 (1991).
14. J. Luettmer-Strathmann, S. Tang, and J. V. Sengers, *J. Chem. Phys.* **97**:2705 (1992).
15. V. Vesovic and W. A. Wakeham, in *Critical Fluid Technology*, T. J. Bruno and J. F. Ely, eds. (CRC Press, Boca Raton, FL, 1991), Chap. 6.
16. A. Eucken, *Phys. Z.* **14**:325 (1913).
17. W. B. Mann and B. G. Dickins, *Proc. Roy. Soc.* **A134**:77 (1931).
18. H. Senftleben and H. Gladisch, *Z. Phys.* **125**:653 (1949).
19. H. Senftleben, *Z. Angew. Phys.* **5**:33 (1953).
20. J. M. Lenoir, W. A. Junk, and E. W. Comings, *Chem. Eng. Prog.* **49**:539 (1953).
21. F. G. Keyes, *Trans. ASME* **76**:809 (1954).
22. R. G. Vines and L. A. Bennett, *J. Chem. Phys.* **22**:360 (1954).
23. J. D. Lambert, K. J. Cotton, M. W. Pailthorpe, A. M. Robinson, J. Scrivins, W. R. F. Vale, and R. M. Young, *Proc. Roy. Soc.* **231A**:280 (1955).
24. D. E. Leng and E. W. Comings, *Ind. Eng. Chem.* **49**:2043 (1957).
25. H. Geier and K. Schäfer, *Allg. Wärmetech.* **10**:70 (1961).
26. H. Senftleben, *Z. Angew. Phys.* **16**:111 (1963); **17**:86 (1964).
27. L. T. Carmichael, V. Berry, and B. H. Sage, *J. Chem. Eng. Data* **8**:281 (1963).
28. Ya. M. Naziev, *Khimya Tekhn. Topl. Masel* **9**:26 (1964).
29. B. Schramm and K. Schäfer, *Ber. Bunsenges Phys. Chem.* **69**:110 (1965).
30. T. Gilmore and E. W. Comings, *AIChE J.* **12**:1173 (1966).
31. B. Le Neindre, R. Tufeu, P. Bury, P. Johannin, and B. Vodar, *Proc. Eighth Conf. Therm. Cond.*, H. Y. Ho and R. E. Taylor, eds. (Plenum Press, New York, 1969), p. 229.
32. B. Le Neindre, *Int. J. Heat Mass Trans.* **15**:1 (1972).
33. N. I. Rjabcev and V. A. Kasarjan, *Study of Thermal Conductivity of Gaseous Hydrocarbons* (VNIIE, Gas Prom., Moscow, 1972) (Russian).
34. A. A. Clifford, E. Dickinson, and P. Gray, *J. Chem. Soc. Faraday Trans. I* **72**:1997 (1976).
35. L. V. Yakush, N. A. Vanicheva, and L. S. Zaitseva, *J. Eng. Phys.* **37**:1071 (1979).
36. R. Fleeter, J. Kestin, and W. A. Wakeham, *Physica* **103A**:521 (1980).
37. R. Tufeu, Y. Garrabos, and B. Le Neindre, *16th Int. Conf. Therm. Conduct.*, D. C. Lapse, ed. (Plenum, New York, 1983), p. 605.

38. R. C. Prasad and J. E. S. Venart, *Int. J. Thermophys.* **5**:367 (1984).
39. X. Y. Zheng, S. Yamamoto, H. Yoshida, H. Masuoka, and M. Yorizane, *J. Chem. Eng. (Jap.)* **17**:237 (1984).
40. H. M. Roder, *National Bureau of Standards Report* 84-3006 (1984).
41. H. M. Roder and C. A. Nieto de Castro, *High Temp.-High Press.* **17**:453 (1985).
42. P. Desmarest and R. Tufeu, *Int. J. Thermophys.* **8**:293 (1987).
43. R. Mostert, H. R. van den Berg, and P. S. van der Gulik, *Int. J. Thermophys.* **10**:409 (1989).
44. W. A. Wakeham and V. Vesovic, in *Status and Future Developments in the Study of Transport Properties*, NATO ASI Series C, W. A. Wakeham, A. S. Dickinson, F. R. W. McCourt, and V. Vesovic, eds. (Kluwer Press, Dordrecht, The Netherlands, 1992), p. 29.
45. CODATA Bulletin No. 63 (1986).
46. V. P. Glushko, L. V. Gurvich, G. A. Bergman, I. V. Veyto, V. A. Medvedev, G. A. Khachkurzov, and Y. S. Youngman, *Thermodynamic Properties of Individual Substances*, 3rd ed. (Nauka, Moscow, 1978).
47. J. P. J. Heemskerk, F. G. van Kuik, H. F. P. Knaap, and J. J. M. Beenakker, *Physica* **71**:484 (1974).
48. J. Millat, A. Plantikow, D. Mathes, and N. H. Nimz, *Z. Phys. Chem. (Leipzig)* **269**:865 (1988).
49. C. C. K. Wong, F. R. W. McCourt, and A. S. Dickinson, *Mol. Phys.* **66**:1235 (1989).
50. A. Michels, J. V. Sengers, and P. S. van der Gulik, *Physica* **28**:1216 (1962).
51. A. M. Sirota, V. I. Latunin, and N. E. Nikolaeva, *Therm. Eng.* **28**:246 (1981) (Russian).
52. B. Le Neindre, Y. Garrabos, and R. Tufeu, *Ber. Bunsenges. Phys. Chem.* **88**:916 (1984).
53. G. A. Olchowy and J. V. Sengers, *Phys. Rev. Lett.* **61**:15 (1988).
54. K. Kawasaki, *Phase Transitions and Critical Phenomena*, C. Domb and M. S. Green, eds. (Academic Press, New York, 1976), Vol. 5A, p. 165.
55. G. A. Olchowy, J. Luettmer-Strathmann, and J. V. Sengers, in preparation.
56. H. C. Burstyn and J. V. Sengers, *Phys. Rev. A* **25**:448 (1982).
57. R. Tufeu, Ph.D. thesis (Université Paris, Paris, 1971).
58. P. Jany and J. Straub, *Int. J. Thermophys.* **8**:165 (1987).
59. K. M. de Reuck and B. Armstrong, *Cryogenics* **19**:505 (1979).
60. M. J. Assael, E. Charitidou, J. H. Dymond, and M. Papadaki, *Int. J. Thermophys.* **13**:237 (1992).